Applied Catalysis B: Environmental 187 (2016) 37–46

Contents lists available at ScienceDirect

Applied Catalysis B: Environmental

journal homepage: www.elsevier.com/locate/apcatb

Highly reactive and selective Sn-Pd bimetallic catalyst supported by nanocrystalline ZSM-5 for aqueous nitrate reduction

Shanawar Hamid [1], Macharla Arun Kumar [1], Woojin Lee *

Department of Civil and Environmental Engineering, Korea Advanced Institute of Science and Technology, 291 Daehak-ro, Yuseong-gu, Daejeon 34141, Republic of Korea

ARTICLE INFO

Article history:
Received 17 September 2015
Received in revised form 12 January 2016
Accepted 13 January 2016
Available online 15 January 2016

Keywords:
Sn-Pd bimetallic catalyst
Nanocrystalline ZSM-5 support
Catalytic nitrate reduction

ABSTRACT

A new bimetallic catalyst supported by environmentally benign nanocrystalline ZSM-5 (NZSM-5), was developed to reduce nitrate completely and selectively to nitrogen gas without producing nitrite. The catalyst was optimized by use under a variety of conditions (i.e., promoter metal type (Sn, Cu, Ag, Ni)), noble metal type (Pd, Pt, Au), promoter metal concentration (0–3.4 wt%), noble metal concentration (0–2.8 wt%), catalyst calcination temperature (0–550 °C), H_2 flow rate (0–60 mL/min), and CO_2 flow rate (0–60 mL/min). Complete nitrate removal with the highest nitrogen selectivity (91%) was achieved using 1%Sn-1.6%Pd-NZSM-5 catalyst under optimized conditions that included: initial nitrate concentration: 30 mg/L NO_3-N; calcination temperature: 350 °C; H_2 flow rate: 30 mL/min; and CO_2 flow rate: 60 mL/min for 60 min. The estimated kinetic rate constant of the catalyst is 16.40×10^{-2} min^{-1}, the catalyst-loading normalized rate constant is 65.60×10^{-2} min^{-1} $g_{cat}{}^{-1}$, while Pd-loading normalized rate constant is 410×10^{-2} L/min $g_{Pd}{}^{-1}$. The catalyst showed remarkable nitrate removal (100%) and nitrogen selectivity (>88%) for up to five successive reactions with consistent kinetics. A 100% nitrate removal and >81% nitrogen selectivity was also achieved by the catalyst for five repeated cycles. However, the kinetics gradually slowed down to 4.36×10^{-2} min^{-1} over five repeated cycles, (still superior to fresh catalysts already reported in the literature). Characterization tests confirmed that the used catalyst was chemically stable, and that the decrease in its reactivity was due mainly to the sintering of metallic nano particles during the regeneration process.

1. Introduction

In recent years, surface and ground waters are increasingly contaminated with nitrate ($NO_3{}^-$) due to anthropogenic activities such as overuse of fertilizer in agriculture, disposal of massive amounts of excrement from livestock, and discharge of poorly treated industrial wastewater [1]. $NO_3{}^-$ contamination is posing serious concerns to human health, ecological cycles, and overall water supply [1–3]. Recently, catalytic $NO_3{}^-$ reduction using supported bimetals has emerged as a promising technology to reduce $NO_3{}^-$ to a harmless end product, nitrogen (N_2). This contrasts with conventional techniques that produce additional sludge and unwanted byproducts, at high operational cost [1–8]. Extensive research has been done to enhance the reactivity and selectivity of bimetallic catalysts using diverse combinations of promoter metals (Cu, Sn, Ag, In and Ni) and noble metals (Pd, Pt, Rh) [1–15]. Among these options, Cu-Pd and Sn-Pd bimetallic catalysts are regarded as very effective combinations [1,4]. In particular, Sn-promoted Pd bimetallic catalyst is superior to Cu-Pd in terms of $NO_3{}^-$ conversion, process selectivity, and byproduct selectivity [4,16]. Numerous materials (e.g., TiO_2 [8], SiO_2 [9,10], Al_2O_3 [11,12], ZrO_2 [13], Fe_2O_3 [1], zero valent Iron [14], activated carbon [15], carbon nanotubes [7], synthetic resins [17] and commercial zeolites [18–20]) have been used to support the bimetals. The use of TiO_2, Al_2O_3, SiO_2, and carbon nanotubes is still controversial due to their potential toxicity to both humans and aquatic life [21–23]. In addition, a high degree of promoter metal leaching has been reported when various metal oxides and metallic-nonmetallic composites have been used as support materials [9,24]. The leaching of promoter and/or noble metals can damage catalyst reactivity and durability; and cause significant impact from toxicity to aquatic life. Some environmentally benign support materials such as iron oxides, for example hematite and maghemite (α- and γ-Fe_2O_3) have also been used for better N_2 selectivity. However the degradation kinetics of these iron-based materials is relatively slow, compared to some of

* Corresponding author.
E-mail addresses: woojin_lee@kaist.edu, woojin_lee@kaist.ac.kr (W. Lee).
[1] These authors contribute equally to this work.

http://dx.doi.org/10.1016/j.apcatb.2016.01.035
0926-3373/

the aforementioned support materials such as Al_2O_3, and SiO_2. The bimetallic catalyst supported by nano-scale zero valent iron (NZVI) is reactive for NO_3^- removal but does not provide high N_2 selectivity and stability over long-term operation [14]. These research results have limited the field application of bimetallic catalysts to treatment of serious NO_3^- contamination problems in natural and engineered water systems. Hence, environmental technology markets still need highly reactive, selective, stable, and eco-friendly catalysts to solve such serious NO_3^-contamination in the water systems.

Zeolites are crystalline microporous aluminosilicates with pore structures consisting of a three dimensional (3D) network of SiO_4 and AlO_4 tetrahedra linked by corners sharing oxygen ions [25]. Catalysts supported by various zeolites have played a significant role in fine chemical and petroleum industries [26,27]. Bimetallic catalyst supported by commercial zeolites like NaY, Beta, and mordenite [18–20] have also shown promising reactivity towards nitrate reduction in aqueous phase. This is due mainly to the fact that zeolites have uniform channel size, unique molecular shape selectivity, and good thermal/hydrothermal stability. Nano-sized zeolite crystals (<100 nm) with narrow particle-size distributions have attracted closer attention for potential application to adsorption and catalytic reactions. The decreased particle size from micro to nano-meter scale leads to substantial changes in the physicochemical properties of the material, commonly resulting in high external surface areas, more exposed active sites, and reduced diffusion path-lengths. Furthermore, the density of pore openings in nanocrystalline zeolites is greater than that in microcrystalline zeolites [28]. Among a variety of zeolites, ZSM-5 has proven a versatile catalytic material for many industrial applications. ZSM-5 is a 3D 10-membered ring zeolite composed of straight and zigzag channels, with a pore diameter of 0.56 nm [29]. In recent years, many attempts have been made to prepare ZSM-5 nanocrystals for study of their activities in various catalytic reactions [30]. Nanocrystalline ZSM-5 (NZSM-5) zeolite could be a good support material for bimetallic catalysts because 1) it can provide excellent dispersion of bimetals due to its high surface area and surface silanol groups, 2) it is insoluble in aqueous solution and stable under extreme thermal and pH conditions, and 3) it is ecofriendly [31]. Due to the unique properties, NZSM-5 was selected as the support material in this study.

The main goal of this work was to develop a novel bimetallic catalyst supported by NZSM-5 for better removal of aqueous NO_3^- and higher N_2 selectivity. The specific objectives were (1) to determine a proper catalyst formulation by optimizing significant factors such as type and contents of promoter and noble metals, calcination temperature, amounts of hydrogen (H_2) and carbon dioxide (CO_2) supply, (2) to elucidate the reaction mechanism of bimetallic catalysis by characterizing fresh and used catalysts using X-ray diffraction (XRD), Furrier Transformation Infrared spectroscopy (FT-IR), scanning electron microscopy with energy dispersive X-ray (SEM/EDX), transmission electron microscopy (TEM/EDX); Brunauer, Emmett, and Teller (BET) specific surface area, Inductively coupled plasma mass spectrometry (ICP-MS), X-ray photoelectron spectroscopy (XPS), and H_2 pulse chemisorption, and (3) investigate the durability and stability of the new optimized bimetallic catalyst (nOBC) by monitoring NO_3^- removal over five cycles.

2. Experimental

2.1. Chemicals

Tetrapropylammonium hydroxide (TPAOH, 20 wt%), tetraethylorthosilicate (TEOS), and aluminum sulfate ($Al_2(SO_4)16H_2O$) were purchased from Sigma-Aldrich Inc. Precursor solutions of Sn, Cu, Ag, Ni, Pd, Pt, and Au were prepared with tin(IV) chloride pentahydrate (98%, Junsei Chemical Co., Japan), copper(II) chloride dehydrate (97.5%, Samchun Pure Chemicals Co., Korea), silver nitrate (99.8%, Samchun Pure Chemicals Co., Korea), nickle(II) chloride hexa hydrate (97%, Samchun Pure Chemicals Co., Korea), palladium(II) chloride (99.9%, Sigma-Aldrich Inc., USA), platinum(IV) chloride (99%, ACROS Organics, USA), and gold(III) chloride trihydrate (99.9%, Sigma–Aldrich Inc., USA), respectively. Sodium borohydride (98.0%, Samchun Pure Chemical Co., Korea) was used to reduce bimetallic catalyst. Potassium nitrite (97.0%, Samchun Pure Chemical Co., Korea), potassium nitrate (99.0%, Duksan Pure Chemical Co., Korea), and ammonium chloride (98.5%, Duksan Pure Chemical Co., Korea) were used for stock and standard solutions for ion chromatography (IC). Sodium bicarbonate (99.7%, Sigma-Aldrich Inc., USA), sodium carbonate (99.95%, Sigma-Aldrich Inc., USA), and nitric acid (60%, OCI Company Ltd, Korea) were used to prepare eluent for IC operation. De-aerated deionized water (DDIW) was prepared with an ultrapure water system (ELGA PURELAB Classic) by purging it with argon gas for 4 h. The DDIW was stored in an anaerobic chamber filled with 95% Ar and 5% H_2 (Coy Laboratory Products, Inc.). All the chemicals used in this study were in as-received form.

2.2. Synthesis of nanocrystalline ZSM-5 zeolite

Aluminum sulfate was added to 20 wt% aqueous solution of TPAOH. Before adding TEOS, the mixture was stirred at 0 °C to obtain a clear solution leading to its molar composition of 1 Al_2O_3:60 SiO_2:21.4 TPAOH. This final mixture was stirred at room temperature for 48 h to hydrolyze TEOS completely. Thereafter, the solution was heated at 80 °C to remove water and alcohols. Finally, the concentrated solution was placed in a Teflon-lined, stainless-steel autoclave, and crystallized by thermal treatment under autogenous pressure and static temperature at 170 °C for 3 days. After this treatment, the solid product was filtered, washed several times with distilled water, dried overnight at 80 °C, and then calcined in air at 550 °C, for 8 h.

2.3. Synthesis of Sn-Pd-NZSM-5

Bimetallic Sn-Pd-NZSM-5 catalysts were synthesized using the modified impregnation method [1]. The NZSM-5 was mixed with 100 mL of DDIW and then subjected to ultrasonic vibration for 6 min, prior to addition of the appropriate amount of Sn and Pd precursors. Pd precursor solution was sonicated for 2 h before its addition. Each Sn and Pd precursor solution was sequentially introduced into the support suspension and mixed under continuous stirring for 2 h. The mixture including Sn and Pd precursors, was dried on a hot plate with continuous stirring at 90 °C. Finally, it was calcined for stabilization of the metals on the surface of NZSM-5 at 350 °C (unless otherwise specified) for 2 h.

Next, the calcined bimetallic catalyst was reduced through the dropwise addition of 0.01 M $NaBH_4$ to completely reduce the Sn and Pd on the support surface [1,6]. The reduced Sn-Pd-NZSM-5 catalysts were vacuum-filtered using a 0.2 μm membrane filter and washed with DDIW twice to remove residual chemicals. The catalyst thus prepared was used immediately for batch experiments. The other experimental catalysts (Cu-Pd-NZSM-5, Ni-Pd-NZSM-5, Ag-Pd-NZSM-5, Sn-Pt-NZSM-5, and Sn-Au-NZSM-5) were prepared using the same method described above.

2.4. Experimental procedure

A batch kinetic test for the catalytic reduction of NO_3^- was performed in a 500 mL glass reactor equipped with a mechani-

cal stirrer, gas inlet and outlet, and two ports for injection and sampling.

In general, a 100 mL DDIW was taken into the reactor and H_2 was bubbled through a glass diffuser in order to remove the dissolved oxygen. After 30 min, a 0.25 g of previously reduced Sn-Pd-NZSM-5 catalyst was added to the reactor. The suspension was continuously stirred at 300 rpm. The catalytic NO_3^- reduction was initiated by the addition of NO_3^- stock solution (20,000 mg/L as NO_3^--N) in order to obtain an initial concentration of 30 mg/L as NO_3-N at room temperature (25 °C). H_2 and CO_2 gases continuously flowed into the reactor to reduce NO_3^- and to keep the suspension at pH 5–6, respectively.

Unless stated otherwise, the experimental conditions were fixed at 2.2 wt% promoter metal, 1.6 wt% noble metal, 30 mL/min H_2, and 40 mL/min CO_2. Batch experiments were conducted to investigate the effect of variation of the promoter metal (Ag, Sn, Cu, and Ni), of noble metal (Pd, Pt, and Au), for five different loadings of Sn (1, 1.6, 2.2, 2.8, and 3.4 wt.%), for five different loadings of Pd (0.4, 1, 1.6, 2.2, and 2.8 wt.%), for four different flow rates of H_2 (15, 30, 45, and 60 mL/min) and for three different flow rates of CO_2 (20, 40, and 60 mL/min); on NO_3^- removal and selectivity of by-products. Catalytic NO_3^- reduction at optimized conditions was evaluated in successive cycles (i.e., without catalyst regeneration). A mixed cellulose ester membrane filter (0.2 μm, Advantech Japan) was attached to the inside of sampling port to avoid catalyst loss and a 2 mL sample was collected at every sampling time by opening sampling port and draining to a falcon tube [14]. After each successive cycle, mixing and H_2 and CO_2 supply were turned off and argon purging started to avoid oxidation of catalyst by atmospheric oxygen. The sampling port was then opened to let the water drain though the filter. Thus, the catalyst was separated without any loss. It was rinsed with DDIW and drained again to remove any residual chemicals. For next successive cycle, DDIW (100 mL) was added to the reactor followed by H_2 and CO_2 purging for 30 min. The reduction was initiated by the addition of NO_3^- stock solution as described above. The NO_3^- removal and selectivity by 1% Sn-1.6% Pd-NZSM-5 during five repeated reaction cycles (i.e., regeneration after every cycle) were also investigated to evaluate its durability and stability for reuse. To regenerate, the 1% Sn-1.6% Pd-NZSM-5 was vacuum-filtered after each reaction cycle to avoid the loss of catalysts. The collected catalyst was washed with DDIW to remove residual ions on the surface, dried at 100 °C for 24 h, calcined at 350 °C, and reduced by $NaBH_4$ as described above. The loss of catalyst after each recycle was compensated by adjusting the volume of DDIW to fix the same catalyst concentration. Likewise, the volume of NO_3^- stock solution was also adjusted to obtain same initial nitrate concentration (30 mg/L NO_3-N) [6]. All experiments were conducted in duplicate. The complete experimental summary along with conditions is given in Supporting information (SI) Table S1.

2.5. Characterization of catalysts

The NZSM-5 supported bimetallic catalyst (Sn-Pd-NZSM-5) was characterized using XRD, FT-IR, SEM/EDX, TEM/EDX, BET, ICP-MS, XPS, and H_2 pulse chemisorption. More details on instrumentation, sample preparation, and analytical procedures are provided in SI.

2.6. Analytical methods

To measure the concentrations of NO_3^-, nitrite (NO_2^-), and ammonium (NH_4^+), an aliquot amount of sample (4 mL) was taken from the reactor using a 5 mL disposable syringe (Korea Vaccine Corp., Korea) at each sampling time. The sample was immediately filtered using a 0.2 μm membrane syringe filter and the concentration of NO_3^-, NO_2^- and NH_4^+ in the filtrate was determined using ion chromatography (IC) (883 basic IC plus, Metrohm, U.K.) equipped with a compact autosampler (863Compact IC, Metrohm, USA), anion column (Metrosep A Supp 4-250/4.0), and cation column (Metrosep C4-150/4.0) [14]. In successive cycles experiments, the concentrations of NO_3^- and NO_2^- were determined by high performance liquid chromatograph (HPLC) (ProStar, Varian, USA), equipped with RP C18 column (Shiseido, Japan) and photodiode array (PDA, 335, Varian, USA) detector at 205 nm, as described elsewhere [1]. The NO_3^- removal (R_{NO3-}) and byproduct selectivity ($S_{byproduct}$), were calculated using the following equations.

$$R_{NO_3^-}(\%) = \frac{[NO_3^- - N]_i - [NO_3^- - N]_f}{[NO_3^- - N]_i}$$

$$S_{NO_2^-}(\%) = \frac{\left[NO_2^- - N\right]_f}{\left[NO_3^- - N\right]_i - \left[NO_3^- - N\right]_f}$$

$$S_{NH_4^+}(\%) = \frac{\left[NH_4^+ - N\right]_f}{\left[NO_3^- - N\right]_i - \left[NO_3^- - N\right]_f}$$

$$S_{N_2^-}(\%) = \frac{\left[NO_3^- - N\right]_i - \left[NO_3^- - N\right]_f - \left[NO_2^- - N\right]_f - \left[NH_4^+ - N\right]_f}{\left[NO_3^- - N\right]_i - \left[NO_3^- - N\right]_f}$$

The subscripts *i* and *f* represent initial and final concentrations, respectively. The by-products other than NH_4^+ and NO_2^- (e.g., NO and N_2O), were negligible in this study [1,5,6]. The Sigma Plot (Systat Software Inc.) was used to calculate the pseudo first order reaction rate constant (*k*, (min^{-1})). The catalyst loading normalized rate constant (K′, ($min^{-1}\ g_{cat}^{-1}$)) was calculated by dividing *k* (min^{-1}) by amount of catalyst used (g), while Pd loading normalized rate constant (K", ($L/min\ g_{Pd}^{-1}$)) was calculated by dividing *k* (min^{-1}) by total Pd content during the reaction ($g_{Pd}\ L^{-1}$).

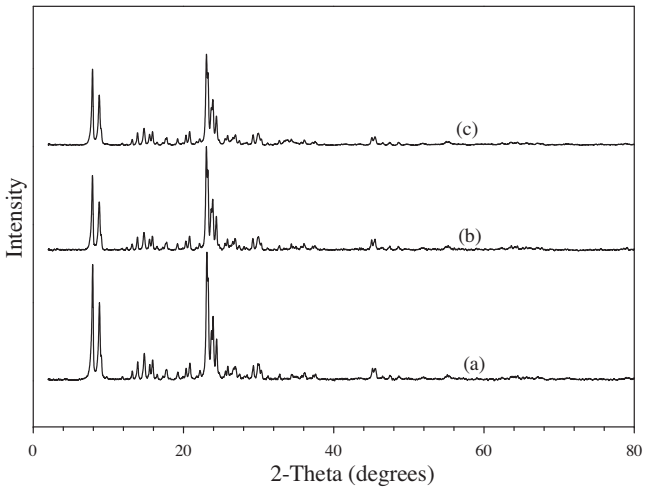

Fig. 1. XRD patterns of (a) NZSM-5 (b) 1% Sn-1.6% Pd-NZSM-5 (fresh) (c) 1% Sn-1.6% Pd-NZSM-5 (after five cycles).

3. Results and discussion

3.1. Catalyst characterization

XRD analysis was performed to verify the crystalline structure of the bimetallic catalyst and its stability during its synthesis and reuse/recycling (Fig. 1). Fig. 1a shows diffraction peaks of synthesized NZSM-5 in the ranges of $2\theta = 7–9°$ and 23–25° corresponding to ZSM-5 structure with high crystallinity [32]. The

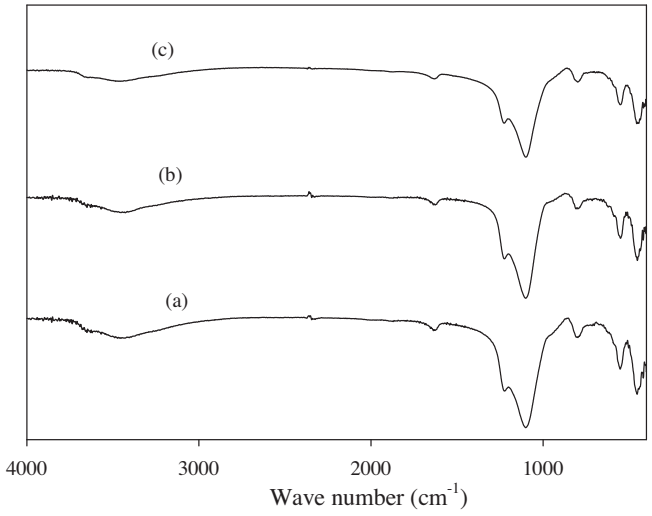

Fig. 2. FT-IR spectra of (a) NZSM-5 (b) 1% Sn-1.6% Pd-NZSM-5 (fresh) (c) 1% Sn-1.6% Pd-NZSM-5 (after five cycles).

average crystalline particle size of the synthesized NZSM-5 estimated by Scherrer's equation was ~27.70 nm. Compared to the XRD pattern of the bare NZSM-5 support, fresh and used catalysts (Fig. 1b and c) showed no obvious change in their diffraction patterns, indicating no change in the crystalline structure of the supports (i.e., NZSM-5 after synthesis, and five cycles run and reuse). The diffraction peaks of Sn and Pd were not observed due to the low content of each metal deposited on the NZSM-5 surface [6,14]. FT-IR analysis was performed to confirm the structural information of the synthesized NZSM-5 zeolite (Fig. 2). The formation of NZSM-5 phase was confirmed by the bands near 1102 cm^{-1} (internal asymmetric stretch), 798 cm^{-1} (external symmetric stretch), 552 cm^{-1} (double ring vibration), and 454 cm^{-1} (T—O bending vibration of the SiO_4 and AlO_4 internal tetrahedral). Additional evidence for its formation was an asymmetric stretch vibration of the band at 1224 cm^{-1}, which is known as a structure-sensitive IR band of ZSM-5 zeolite, and has been assigned to external linkages to TO_4 tetrahedral [33]. No remarkable changes in the FT-IR spectra of fresh and used catalysts was observed, compared to that of NZSM-5. The results from XRD and FT-IR analyses indicate that nano crystalline ZSM-5 was successfully synthesized and it was stable during bimetallic catalyst preparation and five cycles of operation. SEM/EDX analysis was performed to investigate the morphological characteristics of NZSM-5 and dispersion of Sn and Pd on NZSM-5 (Fig. 3 and SI Fig. S1). Fig. 3(a) shows that NZSM-5 particles grew larger aggregates, thereby their primary particle sizes could not easily be determined from the SEM image. The aggregates (100–200 nm) were composed of many nano-sized zeolite particles (20–30 nm). EDX mapping of Sn-Pd-NZSM-5 confirmed the presence of finely dispersed Sn (Fig. 3b-1) and Pd (Fig. 3b-2) particles on the surface of the NZSM-5 matrix. TEM/EDX analysis was also conducted to investigate the detailed morphological characteristics of NZSM-5 and Sn-Pd-NZSM-5 catalyst (Fig. 4 and SI Fig. S2). A TEM image of NZSM-5 (Fig. 4a) shows that the zeolite aggregates formed by the packing of nano-sized (20–30 nm) NZSM-5 particles, were similar to those observed in SEM analysis. A TEM image of Sn-Pd-NZSM-5 (Fig. 4b) shows that many nano-sized (1–5 nm) particles were densely attached to the surface of NZSM-5. The EDX spectra revealed that these were Sn and Pd particles (Fig. 4c). Furthermore, STEM-EDX mapping also revealed that the Sn and Pd were well dispersed on the surface of NZSM-5 (SI Fig. S2). The bimetallic ensembles with size <10 nm were considered as uniformly and densely distributed on the support surface [6,8]. Findings from SEM and TEM analyses showed

Table 1
NO_3^- removal by different combinations of promoter and noble metals on NZSM-5 support.

Promoter metal	Noble metal	NO_3^- removal (%)	k ($10^{-2} \times min^{-1}$)
–	–	0[a]	–
Ni	Pd	30	0.09
Ag	Pd	32	0.13
Cu	Pd	100	2.41
Sn	Pd	100	8.37
Sn	Pt	35	0.15
Sn	Au	16	0.05

[a] Nitrate removal by NZSM-5 only.

that NZSM-5 provided a proper surface for the dense and reasonably uniform dispersion of Sn and Pd, which is a crucial factor for achieving high reactivity of bimetallic catalysts [34].

BET analysis was performed to measure the surface area of NZSM-5 and Sn-Pd-NZSM-5 catalyst. The BET surface area of NZSM-5 was 447 m^2/g, whereas that of Sn-Pd-NZSM-5 was 436 m^2/g. The decrease in surface area of Sn-Pd-NZSM-5 could be due to the incorporation of Sn and Pd on the NZSM-5 surface [35]. SI Table S2 shows that the surface area of NZSM-5 is 1.25–20-times higher than that of materials commonly used as support for NO_3^- reduction (except activated carbon). The surface area of a support could influence the NO_3^- conversion and selectivity of bimetallic catalyst because it can determine the dispersion and availability of active metal sites for NO_3^- reduction [8]. Thus, the greater surface area of NZSM-5 could provide a uniform dispersion of bimetallic particles resulting in high reactivity and selectivity by Sn-Pd-NZSM-5 catalyst.

3.2. Optimization of catalytic NO_3^- reduction by NZSM-5 supported bimetallic catalyst

3.2.1. Effect of different promoter and noble metals on NO_3^- reduction

Table 1 shows NO_3^- removal by bare NZSM-5, Ag-Pd-NZSM-5, Sn-Pd-NZSM-5, Cu-Pd-NZSM-5, and Ni-Pd-NZSM-5 catalysts. The experimental results demonstrate that NO_3^- removal by bare NZSM-5 was negligible, indicating that NZSM-5 was inactive for NO_3^- adsorption or reduction. Sn-Pd-NZSM-5 and Cu-Pd-NZSM-5 showed complete NO_3^- removal (100%), while Ag-Pd-NZSM-5 and Ni-Pd-NZSM-5 showed only 32% and 30% removal, respectively. Results also indicate that reactivity was in the order of Sn > Cu > Ag > Ni. It is well known that the promoter metal can significantly influence the initiation of NO_3^- reduction [36]. In the bimetallic system, NO_3^- is adsorbed on the promoter metal and reduced to NO_2^-, and NO_2^- is then reduced to either N_2 or NH_4^+ (depending on reaction conditions) on the Pd surface. The promoter metal is continuously rejuvenated by spillover of active H species from the noble metal, Pd, keeping the reduction processes running. However, if the promoter metal is permanently oxidized or could not be rejuvenated, NO_3^- reduction slows down and eventually stops. Apparently, Ni and Ag initially reduced by $NaBH_4$ can be exhausted after ~30% NO_3^- reduction and could not have been rejuvenated by H spillover from Pd. Thus, no further reaction proceeded, while the NO_3^- removal by bimetallic catalysts with Sn and Cu proceeded continuously throughout the experiments. The regeneration of Sn and Cu by the H spillover effect is well known during NO_3^- reduction [1,10,14]. The higher reactivity by Sn than by Cu seems to come from the NZSM-5 support providing a more suitable surficial environment for NO_3^- reduction (more explanation is given in Section 3.2.2). Hence, Sn was selected as the representative promoter metal for the next experiments due to its superior NO_3^- reduction kinetics.

Table 1 also shows the NO_3^- reduction kinetics of Sn-Pd-NZMS-5, Sn-Pt-NZSM-5 and Sn-Au-NZSM-5 catalysts. Sn-Pd-NZSM-5

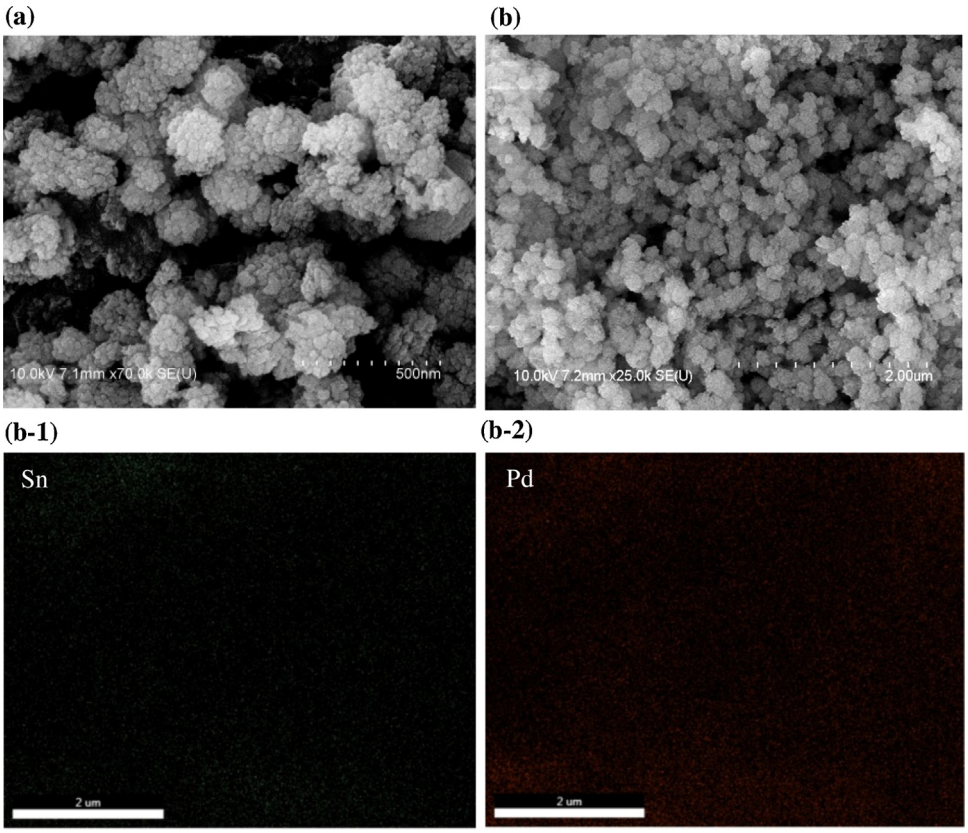

Fig. 3. SEM images of (a) NZSM-5, (b) 1% Sn-1.6% Pd-NZSM-5 (fresh) and elemental maps of (b-1) Sn and (b-2) Pd in 1% Sn-1.6% Pd-NZSM-5 (fresh).

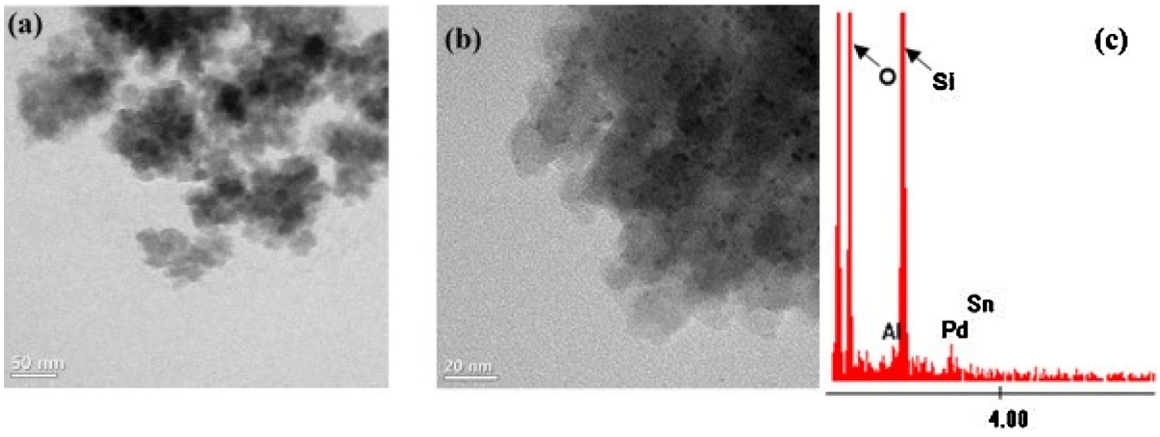

Fig. 4. TEM images of (a) NZSM-5 (b) 1% Sn-1.6% Pd-NZSM-5 (fresh) and (c) EDX spectra of 1% Sn-1.6% Pd-NZSM-5 (fresh).

showed complete NO_3^- removal, while Sn-Pt-NZSM-5 and Sn-Au-NZSM-5 showed only 35% and 16% removal, respectively. Among these three, the catalytic reactivity was in the order Pd > Pt > Au. The higher removal by the Sn-Pd combination is because Pd has a higher H_2 adsorption capacity than do other noble metals [1,6,14,37,38]. The experimental results from the optimization of promoter and noble metal, indicated that Sn-Pd is the most effective combination among the NZSM-5 supported bimetallic catalysts.

3.2.2. *Effect of Sn loading on NO_3^- reduction and selectivity*

Fig. 5 and SI Fig. S3 show the NO_3^- removal and transformation-product selectivity by Sn-Pd-NZSM-5 catalyst at different Sn loadings (0, 1, 1.6, 2.2, 2.8, and 3.4 wt%) in 60 min. No NO_3^- reduction was observed at 0% Sn loading, while >99% NO_3^- was successfully removed by all Sn loadings within 60 min. The kinetic rate constant (k) increased with the increase in Sn content (from 7.75×10^{-2} min^{-1} at 1% Sn, to 10.97×10^{-2} min^{-1} at 3.4% Sn), showing that reactivity of Sn-Pd-NZSM-5 catalyst increased with the increase in Sn loading. The N_2 selectivity decreased with the increase in Sn loading. Interestingly, NO_2^- was not detected during all experiments. These results contradict the experimental trends reported in the literature for both Sn-Pd and Cu-Pd bimetallic catalysts. It has been reported that an increase in promoter metal loading beyond a certain level, negatively affects active surface area of the noble metal due to overlap by the promoter metal [1,6,14]. The loss of active surface area of noble metal results in the decrease of active H species on its surface. Consequently, this can diminish the chances of active H spillover from noble

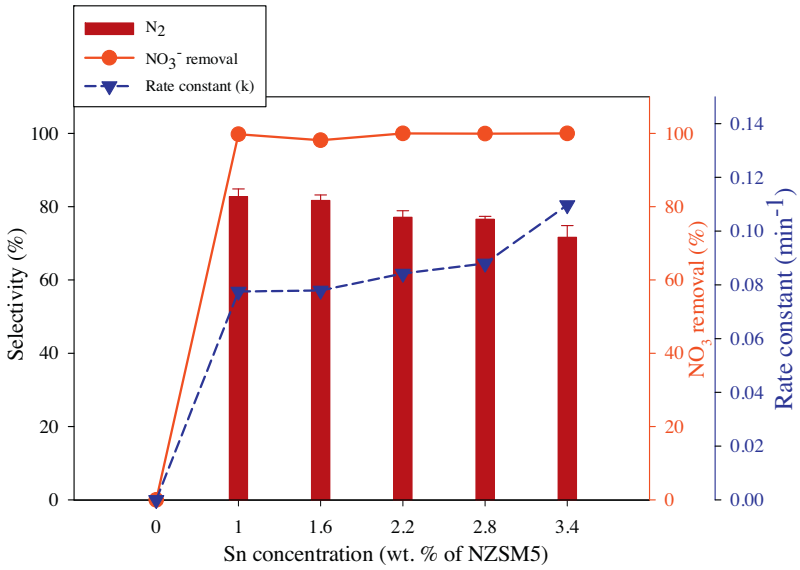

Fig. 5. N_2 selectivity and NO_3^- removal by X% Sn-1.6% Pd-NZMS-5 (X = 0, 1, 1.6, 2.2, 2.8, and 3.4). Conditions: NO_3^- loading: 30 mg/L NO_3-N; catalyst loading: 2.5 g/L; H_2 flow rate: 30 mL/min; CO_2 flow rate: 40 mL/min; calcination temperature: 350 °C; reaction time: 60 min.

metal to promoter metal and slow down NO_3^- reduction kinetics. The decrease of active H spillover also enhances NO_2^- selectivity due to its incomplete reduction process [1,6,14,38]. However, the enhanced NO_3^- degradation kinetics and zero selectivity toward NO_2^- obtained in this study indicate that the NZSM-5 support provided a surface environment suitable for the bimetallic catalyst to achieve complete NO_3^- removal and faster reaction kinetics. Highly crystalline NZSM-5 has higher surface area (447 m^2/g) than other widely reported support materials (e.g., Al_2O_3 (196 m^2/g), TiO_2 (50 m^2/g), zero-valent iron (0.51 m^2/g), and Fe_2O_3 (21 m^2/g). Therefore, increase in Sn loading enhanced the proximity of Sn and Pd, and the quantity of bimetallic ensembles per unit surface area, without overlapping even at higher Sn loading. This ultimately accelerated the NO_3^- reduction kinetics. An enhancement in NH_4^+ selectivity (17% at 1% Sn loading to 29% at 3.4%) could be due to 1) decrease in Pd sites compared to Sn which might lead to the formation of N—H rather than that of N—N [1], and 2) increase in suspension pH (5.8 at 1% Sn loading to 7.5 at 3.5% Sn) due to an increase in NO_3^- reduction rate (7.75×10^{-2} min^{-1} at 1% Sn loading to 10.97×10^{-2} min^{-1} at 3.4%) and limited buffering capacity by the fixed CO_2 supply (40 mg/L) [39]. Hence 1% Sn loading can provide optimal NO_3^- removal (100%) and N_2 selectivity (83%).

3.2.3. *Effect of Pd loading on NO_3^- reduction and selectivity*

Fig. 6 and SI Fig. S4 show the NO_3^- removal and transformation-product selectivity by Sn-Pd-NZSM5 catalyst at different Pd loadings (0, 0.4, 1, 1.6, 2.2, and 2.8 wt%) in 60 min. NO_3^- reduction was not observed at 0% Pd loading, while it increased from 36 to >99% with increase in Pd loading from 0.4 to ≥1.6%. This is due to the increase in Pd loading because this increased the number of reactive sites for the activation of H_2 molecules on the Pd surface ($H_2 + Pd^\circ \rightarrow 2H_{ads} + Pd^\circ$). Thus, it facilitates continuous and swift rejuvenation of SnO_x to Sn° by increased H_{ads} spillover from numerous Pd sites ($SnO_x + H_{ads} \rightarrow Sn^\circ + OH^-$), leading to enhancement of NO_3^- reduction. The N_2 selectivity decreased from 94 to 76% with increase in Pd loading from 0.4 to 2.8%, while NH_4^+ selectivity increased from 6 to 24%. The increase in reactive H species due to increase in Pd loading lowers the N:H ratio. A low N:H ratio facilitates N—H recombination to form NH_4^+, while a high N:H ratio favors N_2 formation [1,5,6,14,39,40]. Accordingly, in this study it was found that NH_4^+ selectivity increased, while N_2 selectivity decreased, with increased

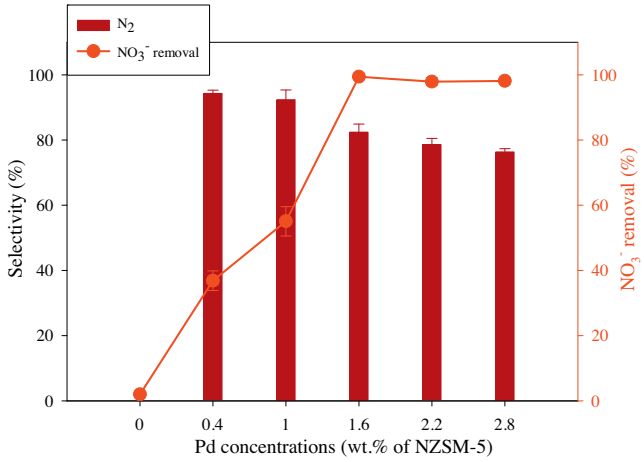

Fig. 6. N_2 selectivity and NO_3^- removal by 1% Sn-X% Pd-NZSM-5 (X = 0, 0.4, 1, 1.6, 2.2, and 2.8). Conditions: NO_3^- loading: 30 mg/L NO_3-N; catalyst loading: 2.5 g/L; H_2 flow rate: 30 mL/min; CO_2 flow rate: 40 mL/min; calcination temperature: 350 °C; reaction time: 60 min.

Pd loading. In this study, 1.6% Pd loading seems to be optimal to activate enough H_2 for complete NO_3^- reduction and high N_2 selectivity (83%). The experimental results show that the increase in Pd loading of Sn-Pd-NZSM-5 catalyst enhances NO_3^- reduction but inhibits the formation of N_2 from NO_2^- reduction.

The reactivity and selectivity of the catalyst was further enhanced by optimizing the effect of calcination temperature, H_2 and CO_2 supplies, and catalyst loading. The experimental results are thoroughly described and discussed in SI (S2.3 - S2.6, Fig. S5 - Fig. S11).

3.3. *Reaction mechanism of NO_3^- reduction on Sn-Pd-NZSM-5 catalyst*

Several control and reduction experiments were performed to elucidate the reaction mechanism of NO_3^- reduction on the surface of Sn-Pd-NZSM-5 bimetallic catalyst. The results are shown in SI Fig. S12. Adsorption or reduction of NO_3^-, NO_2^-, and NH_4^+ on reduced, bare NZSM-5 surfaces was negligible (SI Fig. S12). Control experiments also showed that reduction of NO_3^- on reduced

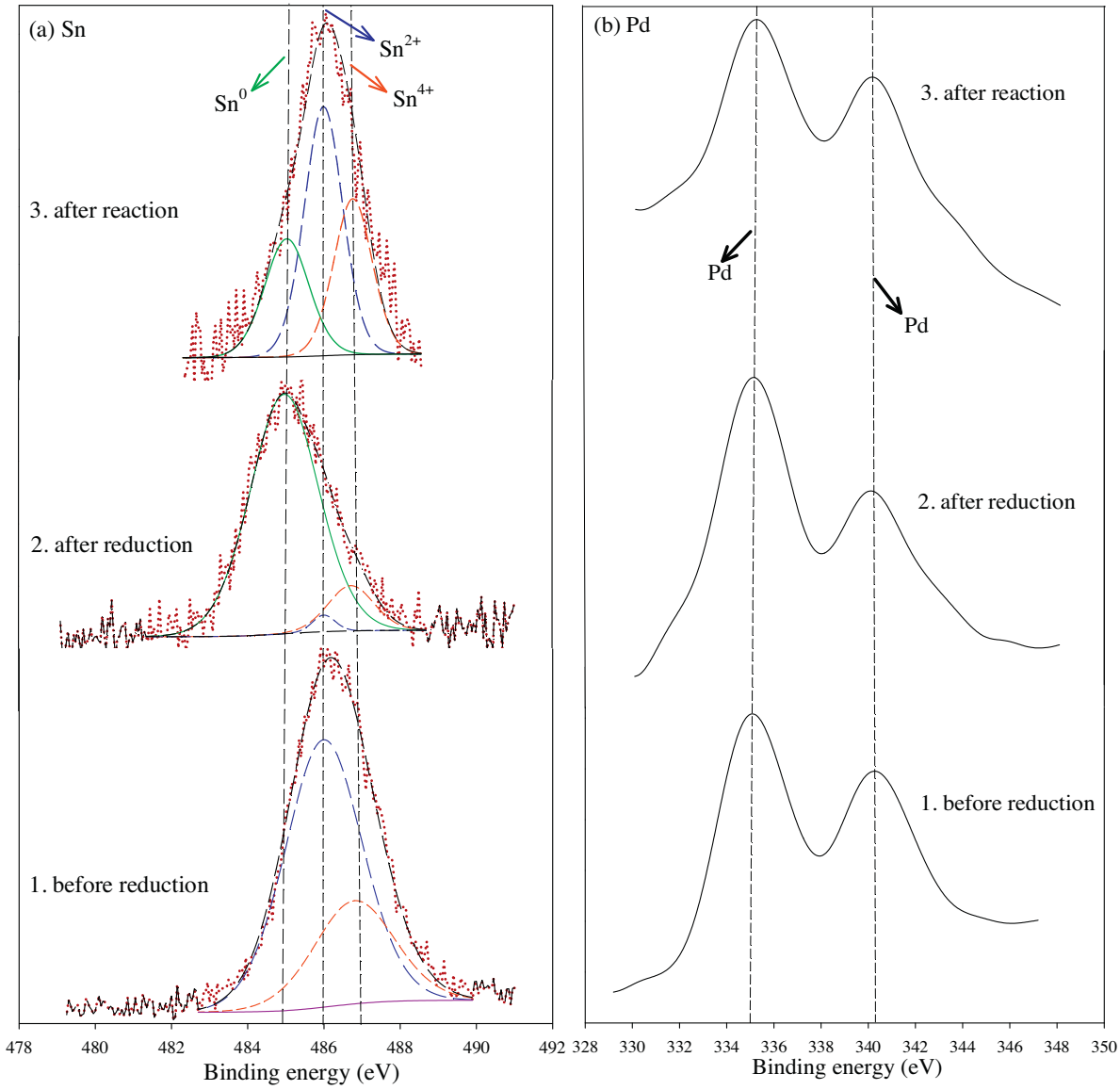

Fig. 7. XPS spectra of (a) Sn (3d5/2) and (b) Pd(3d) on 1% Sn-1.6% Pd-NZSM-5 (fresh).

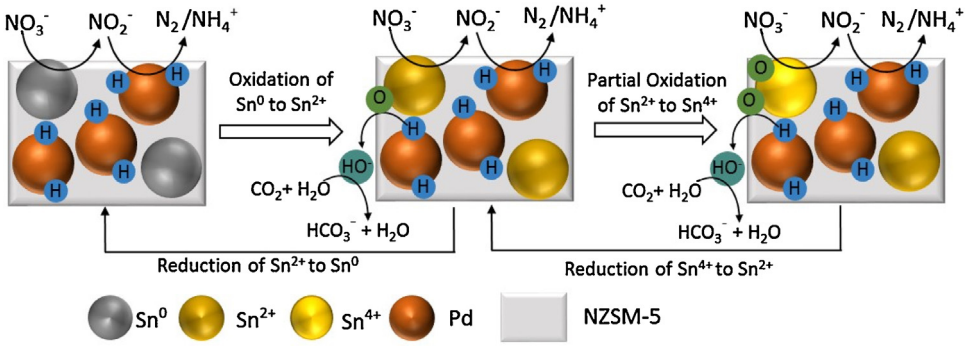

Scheme 1. NO_3^- reduction mechanism on Sn-Pd-NZSM-5 catalyst.

Sn-NZSM-5 and Pd-NZSM-5 monometallic catalysts was negligible, revealing that the monometallic catalysts are lacking in the capacity to induce a significant NO_3^- reduction. A bimetallic catalyst (1% Sn-1.6% Pd-NZSM-5) showed fast and complete NO_3^- removal with selectivity of 91% for N_2 and 9% for NH_4^+, indicating that catalytic nitrate reduction is strongly dependent on the use of reduced Sn-Pd bimetallic ensembles. XPS analysis was conducted to investigate the oxidation states of Pd and Sn before and after reduction with $NaBH_4$ and after NO_3^- reduction reaction (Fig. 7). A narrow scan of Sn(3d5/2) before reduction with $NaBH_4$ revealed two main peaks at

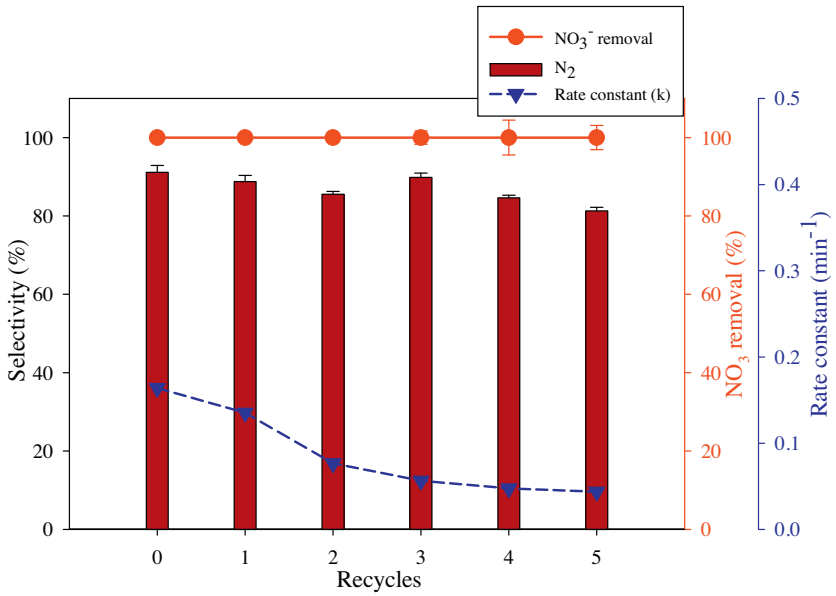

Fig. 8. N_2 selectivity and NO_3^- removal by 1% Sn-1.6% Pd-NZMS-5 during five repeated cycles. Conditions: NO_3^- loading: 30 mg/L NO_3-N; catalyst loading: 2.5 g/L; H_2 flow rate: 30 mL/min; CO_2 flow rate: 60 mL/min; calcination temperature: 350 °C; reaction time: 75 min.

486 and 486.7 eV corresponding to Sn^{2+} (71.24%) and Sn^{4+} (28.76%), respectively (Fig. 7(a) 1 and SI Table S3). This indicated that Sn was present in two oxidation states before its reduction. In contrast, a narrow scan of Sn(3d5/2) after reduction with $NaBH_4$ showed three peaks at 485, 486 and 486.7 eV, corresponding to Sn^0 (86.83%), Sn^{2+} (2.04%) and Sn^{4+} (11.12%), respectively (Fig. 7(a) 2 and SI Table S3). The presence of Sn^{2+} (2.04%) and Sn^{4+} (11.12%) in the reduced catalyst before NO_3^- reduction, could be due to the oxidation of Sn° by atmospheric oxygen during the analysis, or due to issues related to handling the XPS sample holder [1,14]. The presence of Sn^{2+} and Sn^{4+} in fresh catalyst, and that of Sn° in reduced catalyst, suggest that NO_3^- reduction on active Sn surfaces could proceed in two subsequent reduction steps. First, Sn^0 surfaces could reduce NO_3^- and be oxidized to Sn^{2+} (Eq. (1)), and second, Sn^{2+} could be partially oxidized to Sn^{4+} for the reduction (Eq. (2)). This was confirmed by the narrow scan of Sn(3d5/2) after NO_3^- reduction (Fig. 7(a)3 and SI Table S3), which reveals that Sn^0 decreased to 25.22%, while Sn^{2+} and Sn^{4+} increased to 45.98% and 28.8%, respectively, during the NO_3^- reduction.

$$NO_3^- + Sn^0 \rightarrow SnO + NO_2^- \quad (1)$$

$$NO_3^- + SnO \rightarrow SnO_2 + NO_2^- \quad (2)$$

The equations suggest higher NO_2^- production due to higher NO_3^- reduction. Unlike experimental results reported in the literature [1,6,14], NO_2^- was not observed during the reduction tests under optimal conditions, implying that NO_2^- was reduced at a kinetic rate greater than or equal to that of NO_3^- removal (i.e., $\geq 16.40 \times 10^{-2}$ min^{-1}). To verify this hypothesis, a control test was performed by reducing 30 mg/L NO_2-N (same concentration as initial NO_3-N) under the same optimal conditions (i.e., 1% Sn, 1.6% Pd, 30 mL/min H_2, and 60 mL/min CO_2 flow rate). Surprisingly, NO_2^- was completely removed (100%) at a reduction rate of 26.1×10^{-2} min^{-1}, which is 1.6 times higher than that of NO_3^- (16.40×10^{-2} min^{-1}). It is well known that NO_2^- cannot be adsorbed and reduced on the promoter metal surface [1,6]. Instead, it is reduced to NH_4^+ or N_2 by spillover H adsorbed and activated on Pd surfaces. A narrow scan of fresh catalyst for Pd(3d) before and after reduction, revealed that Pd was present only in Pd^0 form (Fig. 7b). This suggests that H_2 can be continuously adsorbed and activated by Pd^0 [14]. Thus, NO_2^- was not observed during NO_3^- reduction because it was continuously and instantaneously reduced to N_2 or NH_4^+ due to high spillover of active H from Pd^0, as shown in Eqs. (3) and (4) (overall NO_2^- reduction).

$$2NO_2^- + 4H_{ads}\text{-}Pd^0 \rightarrow Pd^0 + N_2 + 4OH^- \quad (3.1)$$

$$NO_2^- + 6H_{ads}\text{-}Pd^0 \rightarrow Pd^0 + NH_4^+ + 2OH^- \quad (3.2)$$

$$3NO_2^- + 10H_{ads}\text{-}Pd^0 \rightarrow Pd^0 + N_2 + NH_4^+ + 6OH^- \quad (4)$$

$$3H_{ads}\text{-}Pd^\circ + SnO + SnO_2 \rightarrow 2Sn^0 + Pd^0 + 3OH^- \quad (5)$$

A reaction mechanism for the reduction of nitrate by 1% Sn-1.6% Pd-NZSM-5 under optimal conditions is summarized in Scheme 1, depicting the overall NO_3^- reduction steps in Eqs. (1)–(4). The spillover of activated H from Pd surfaces not only reduces NO_2^- but also rejuvenates SnO and SnO_2 to Sn°, by abstracting oxygen atoms to produce OH^- (Eqs. (3)–(5)). The OH^- produced during the reaction can be buffered by CO_2 to maintain constant and proper pH of the catalyst suspension. The continuous consumption of active H species by fast reduction of NO_2^- and rejuvenation of SnO and SnO_2 may cause a limiting condition for the reaction due to the limited supply of H_2 at 30 mL/min. Under the limiting condition at low pH, N—H recombination can be severely suppressed, whereas N—N recombination can be enhanced to produce more N_2. Hence, this is the reason how 1% Sn-1.6% Pd-NZSM-5 can achieve complete NO_3^- removal with selectivity of 91% for N_2 and only 9% for NH_4^+, one of the best records under all the experimental conditions.

3.4. Recycling of Sn-Pd-NZSM-5 for catalytic NO_3^- reduction

We investigated the catalytic performance of nOBC over five successive cycles without regeneration and then two successive cycles after regeneration and presented its results in SI Fig. S13. nOBC successfully reduced NO_3^- with consistent reactivity ($k = 15.60 \pm 0.90 \times 10^{-2}$ min^{-1}) and selectivities (N_2 ~90%) in all successive reactions, showing that 1% Sn-1.6% Pd-NZSM-5 catalyst is stable and efficient in successive cycles of use.

The nOBC was further evaluated for 5 repeated cycles under optimal conditions to investigate the stability over reuse (Fig. 8). Complete NO_3^- removal was observed by all repeated cycles. NO_2^- production was not observed throughout the recycling experiments. The NH_4^+ selectivity varied from 9 to 19%, while N_2

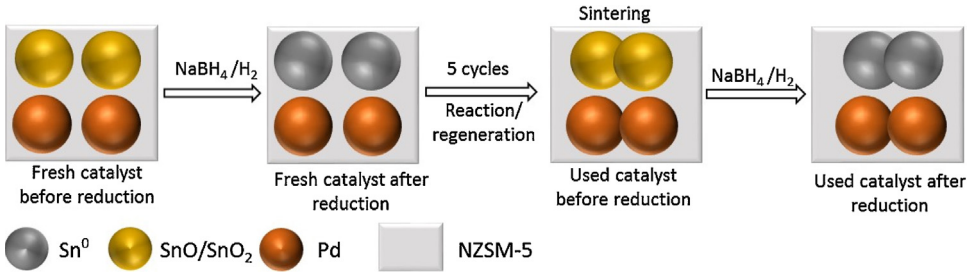

Scheme 2. Sintering of Sn and Pd on NZSM-5 surface during recycling.

Table 2
H_2 pulse chemisorption of fresh and used catalysts.

Catalyst	H_2 cumulative uptake quantity (cm^3/g)	Metal dispersion (%)	Metallic surface area (m^2 per g metal)	Active particle diameter (nm)	Cubic crystallite size (nm)	Active metal sites (10^{-2} mmol)	NO_3^- conversion rate (10^{-5} mmols^1)	TOFNO_3^- (10^{-3} s^{-1})
Fresh	0.35	20.75	92.42	5.40	4.51	1.20	11.94	9.81
After five cycles	0.19	11.44	50.95	9.80	8.16	0.70	5.83	8.68

selectivity varied from 91 to 81% during the repeated cycles. The k value was highest with fresh catalyst (16.40×10^{-2} min^{-1}) and gradually decreased to 4.36×10^{-2} min^{-1} at the fifth cycle.

To investigate factors leading to the decrease in reactivity of the nOBC during the repeated cycles, we employed several characterization and verification tools. ICP/MS analysis was performed to evaluate the leaching of Pd and Sn after each cycle. Negligible leaching of Pd (<0.01%) and Sn (<0.03%) was observed in this study, compared to leaching of promoter metal from bimetallic catalyst supported by SiO_2 (10.60%), Al_2O_3 (30.70%), ZrO_2 (26%), CeO_2 (56.40%), MnO_2 (2.50%), A C-Ce composite (18.10%) and CNT-TiO_2 composite (15.90%) in other studies [9,24]. This indicates that the catalyst was stable during the five cycles of NO_3^- reduction, and that the decline of catalyst reactivity throughout the repeated cycles was not due to the leaching of bimetals from the zeolite support.

XPS analysis of the nOBC after five cycles was also performed to investigate the oxidation states of Sn and Pd (SI Fig. S14 and SI Table S3). The XPS spectra of Sn(3d5/2) after reduction of the sample, showed three peaks corresponding to Sn° (82.59%), Sn^{2+} (6.34%), and Sn^{4+} (11.07%), which are very similar to those in fresh catalyst (SI Table S3). Pd was also found in zero valent metallic form (Pd°) in all cases. The XPS results confirmed that the oxidation states of Sn and Pd were consistent throughout the repeated cycles, showing the potential durability and constant reactivity of the catalyst. SEM-EDX analysis was performed to investigate morphological changes caused by bimetal dispersion after five cycles (SI Fig. S15). The results showed that Sn and Pd aggregated onto NZSM-5 surfaces due to sintering during repeated cycling/regeneration. This was confirmed by STEM-EDX analysis (SI Fig. S16). Bimetals could aggregate during NO_3^- reduction to form bigger particles [6,34]. The sintering of bimetals could disturb the proper proximity of Sn-Pd ensembles, thereby decreasing the surface areas of active metal, and thus H_2 adsorption on Pd surfaces. To verify this, H_2 pulse chemisorption was performed on fresh and fifth cycled catalysts (Table 1). The results confirmed the decrease in active metal dispersion (20.75 to 11.44%), active metal surface area (92.42 to 50.95 m^2/g), cumulative H_2 uptake (0.35 to 0.19 cm^3/g), and increase in active metal particle size (from 4.5 to 9.8 nm), all of which support the evidence of metal particle sintering as depicted in Scheme 2. Based on these results, the turnover frequency (TOF) of fresh and fifth-cycle catalysts was calculated. From this, it was determined that TOF decreased from 9.81×10^{-3} s^{-1} to 8.68×10^{-3} s^{-1} over five cycles (Table 2). The TOF determines the reactivity, and it is helpful for comparing the performance of catalysts regardless of the specific conditions. Decrease in TOF indicates that the reactivity of the nOBC slowed down due to sintering, so more time was needed to reduce the NO_3^- completely, than would be needed using fresh catalyst. However, it is worth mentioning that the TOF of the five-cycle Sn-Pd-NZSM-5 catalyst (8.68×10^{-3} s^{-1}) is still 6–18 times higher than fresh bimetallic catalysts supported by SiO_2 (0.47×10^{-3} s^{-1}), CeO_2 (0.53×10^{-3} s^{-1}), Al_2O_3 (1.14×10^{-3} s^{-1}), and α-Fe_2O_3 (1.53×10^{-3} s^{-1}) [1]. This clearly indicates the superior reactivity of the catalyst developed in this study.

The results from SEM, STEM, and H_2 pulse chemisorption analyses support the hypothesis that the decrease in the reactivity of the optimized Sn-Pd-NZSM-5 catalyst was due mainly to the sintering of Sn and Pd during repeated cycles and regeneration steps. However, the superior reaction kinetics and high selectivity of fresh and used Sn-Pd-NZSM-5 catalyst, in comparison to those reported in the literature (SI Table S2 and SI Fig. S17) indicate that the optimized Sn-Pd-NZSM-5 is the most effective and selective bimetallic catalyst, and has remarkable stability and durability for reduction of NO_3^-.

4. Conclusion

In this study, we developed an effective, stable, and recyclable Sn-Pd bimetallic catalyst supported by NZSM-5 for complete NO_3^- removal, with high selectivity toward N_2 and without NO_2^- accumulation. The reaction kinetics of NO_3^- reduction by the optimized Sn-Pd-NZSM-5 catalyst ($k = 16.40 \times 10^{-2}$ min^{-1}, $K' = 65.60 \times 10^{-2}$ min^{-1} $g_{cat}{}^{-1}$, $K'' = 410 \times 10^{-2}$ L min^{-1} $g_{Pd}{}^{-1}$) obtained in this study is one of the fastest reaction kinetics among those of catalysts reported in the literature, despite its low metal loading and catalyst content (SI Table S2). The exceptional reactivity and selectivity of the optimized Sn-Pd-NZSM-5 certainly are due to 1) the excellent support properties of NZSM-5, which provides a surface appropriate for uniform dispersion of Sn and Pd; 2) subsequent electron transfer from Sn° and Sn^{2+} sites to reduce more NO_3^-; 3) continuous rejuvenation of oxidized Sn by enhanced H spillover from Pd sites; and 4) CO_2 buffering to keep the suspension-pH constant by consuming OH^- during the reaction. The nOBC showed continuous remarkable NO_3^- removal with fast reaction kinetics and high N_2 selectivity (>88%) throughout five successive reaction cycles. We also believe that this new optimized bimetallic catalyst (Sn-Pd-NZSM-5) is the first catalyst to show complete NO_3^- removal and high level of selectivity for N_2 (>81%), for up to five repeated cycles under experimental condi-

tions. The structure of the catalyst support after five cycles was very similar to that of a fresh one, and the leaching of Sn and Pd from the catalyst surface was negligible during the repeated reactions and regeneration steps. For these reasons, we conclude that this optimized Sn-Pd-NZSM-5 is a robust, stable, and durable catalyst for selective and sustainable denitrification processes. These results can provide novel and basic knowledge helpful for solving difficult problems of nitrogen removal in biological wastewater treatment plants, and applicable for use by ex-situ remediation facilities to treat groundwater severely contaminated by nitrate.

Acknowledgements

This work was financially supported by research grants from the Korean Ministry of Environment, GAIA project (173-111-036), other GAIA project (RE201402059), and the National Research Foundation of Korea (NRF) funded by the Ministry of Education (2012-C1AAA001-M1A2A2026588).

Appendix A. Supplementary data

Supplementary data associated with this article can be found, in the online version, at http://dx.doi.org/10.1016/j.apcatb.2016.01.035.

References

[1] S. Jung, S. Bae, W. Lee, Environ. Sci. Technol. 48 (2014) 9651.
[2] A. Pintar, Catal. Today 77 (2003) 451.
[3] H. Shin, S. Jung, S. Bae, W. Lee, H. Kim, Environ. Sci. Technol. 48 (2014) 12768.
[4] U. Prusse, M. Hahnlein, J. Daum, K.D. Vorlop, Catal. Today 55 (2000) 79.
[5] Y.H. Liou, C.J. Lin, S.C. Weng, H.H. Ou, S.L. Lo, Environ. Sci. Technol. 43 (2009) 2482.
[6] J. Jung, S. Bae, W. Lee, Appl. Catal. B: Environ. 127 (2012) 148.
[7] O.S.G.P. Soares, J.J.M. Órfa, E. Gallegos-Suarez, E. Castillejos, I. Rodríguez-Ramos, M.F.R. Pereira, Environ. Technol. 33 (2012) 2353.
[8] W. Gao, N. Guan, J. Chen, X. Guan, R. Jin, H. Zeng, Z. Liu, F. Zhang, Appl. Catal. B: Environ. 46 (2003) 341.
[9] Y. Yoshinaga, T. Akita, I. Mikami, T. Okuhara, J. Catal. 207 (2002) 37.
[10] A. Garron, K. Lazar, F. Epron, Appl. Catal. B: Environ. 59 (2005) 57.
[11] C.L. Constantinou, C.N. Costa, A.M. Efstathiou, Environ. Sci. Technol. 41 (2007) 950.
[12] J. Batista, A. Pintar, D. Mandrino, M. Jenko, V. Martin, Appl. Catal. A: Gen. 206 (2001) 113.
[13] Z. Xu, L. Chen, Y. Shao, D. Yin, S. Zheng, Ind. Eng. Chem. Res. 48 (2009) 8356.
[14] S. Hamid, S. Bae, W. Lee, M.T. Amin, A.A. Alazba, Ind. Eng. Chem. Res. 54 (2015) 6247.
[15] O.S.G.P. Soares, J.J.M. Orfao, J. Ruiz-Martinez, J. Silvestre-Albero, A. Sepulveda-Escribano, M.F.R. Pereira, Chem. Eng. J. 165 (2010) 78.
[16] J. Sa, D. Gasparovicova, K. Hayek, E. Halwax, J.A. Anderson, H. Venek, Catal. Lett. 105 (2005) 209.
[17] D. Gasparovicova, M. Kralik, M. Hronec, Z. Vallusova, H. Vinek, B. Corain, J. Mol. Catal. A: Chem. 264 (2007) 93.
[18] O.S.G.P. Soares, L. Marques, C.M.A.S. Freitas, A.M. Fonseca, P. Parpot, J.J.M. Órfão, M.F.R. Pereira, I.C. Neves, Chem. Eng. J. 281 (2015) 411.
[19] K. Nakamura, Y. Yoshida, I. Mikami, T. Okuhara, Chem. Lett. 34 (2005) 678.
[20] K. Nakamura, Y. Yoshida, I. Mikami, T. Okuhara, Appl. Catal. B: Environ. 65 (2006) 31.
[21] X. Zhu, Y. Chang, Y. Chen, Chemosphere 78 (2010) 209.
[22] A. Simon-Deckers, B. Gouget, M. Mayne-L'Hermite, N. Herlin-Boime, C. Reynaud, M. Carrière, Toxicology. 253 (2008) 137.
[23] W. Lin, Y.W. Huang, X.D. Zhou, Y. Ma, Toxicol. Appl. Pharm. 217 (2006) 252.
[24] O.S.G.P. Soares, J.J.M. Órfão, M.F.R. Pereira, Desalination 279 (2011) 367.
[25] A. Dyer, An Introduction to Zeolite Molecular Sieves, Wiley, Chichester, 1988.
[26] C.S. Cundy, P.A. Cox, Chem. Rev. 103 (2003) 663.
[27] A. Primo, H. Garcia, Chem. Soc. Rev. 43 (2014) 7548.
[28] T. Tago, K. Iwakai, M. Nishi, T. Masuda, J. Nanosci. Nanotechnol. 9 (2009) 612.
[29] W. Song, R.E. Justice, C.A. Jones, V.H. Grassian, S.C. Larsen, Langmuir 20 (2004) 8301.
[30] K. Shen, N. Wang, W. Qian, Y. Cui, F. Wei, Catal. Sci. Technol. 4 (2014) 3840.
[31] S. Narayanan, J.J. Vijaya, S. Sivasanker, L.J. Kennedy, A. Ariharan, J. Porous Mater. 21 (2014) 633–641.
[32] D.W. Breck, Zeolite Molecular Sieves, Willey, New York, 1974.
[33] Y. Chang, L. Jun, J.S. Li, Y.C. Yang, X.Y. Sun, Mater. Lett. 59 (2005) 3427.
[34] Y. Xie, H. Cao, Y. Li, Y. Zhang, J.C. Crittenden, Environ. Sci. Technol. 45 (2011) 4066.
[35] A. Devadas, S. Vasudevan, F. Epron, J. Hazard. Mater. 185 (2011) 1412.
[36] N. Barrabes, J. Sa, Appl. Catal. B: Environ. 104 (2011) 1.
[37] N. Barrabes, J. Just, A. Dafinov, F. Medina, J.L.G. Fierro, J.E. Sueiras, P. Salagre, Y. Cesteros, Appl. Catal. B: Environ. 62 (2006) 77.
[38] H. Berndt, I. Mönnich, B. Lücke, M. Menzel, Appl. Catal. B: Environ. 30 (2001) 111.
[39] R. Gavagnin, L. Basetto, F. Pinna, G. Strukul, Appl. Catal. B: Environ. 38 (2002) 91.
[40] T.C. Zhang, Y.H. Huang, J. Energy Eng. 131 (2005) 461.